Measurements of optical Feshbach resonances of ^{174}Yb atoms

Min-Seok Kim,[1] Jeongwon Lee,[2] Jae Hoon Lee,[2] Y. Shin,[1,3] and Jongchul Mun[2,*]
[1]*Department of Physics and Astronomy, and Institute of Applied Physics, Seoul National University, Seoul 08826, Korea*
[2]*Korea Research Institute of Standards and Science, Daejeon 34113, Korea*
[3]*Center for Correlated Electron Systems, Institute for Basic Science, Seoul 08826, Korea*
(Received 11 July 2016; published 10 October 2016)

We present measurements of the optical Feshbach resonances (OFRs) of ^{174}Yb atoms for the intercombination transition. We measure the photoassociation (PA) spectra of a pure ^{174}Yb Bose-Einstein condensate (BEC) and determine the dependence of OFRs on PA laser intensities and frequencies for four least-bound vibrational levels near the intercombination transition. We confirm that our measurements are consistent with the temporal decay of a BEC subjected to a PA beam in the vicinity of the fourth vibrational level from the dissociation limit.

DOI: 10.1103/PhysRevA.94.042703

I. INTRODUCTION

A Feshbach resonance (FR) arises when a bound molecular state energetically reaches a scattering state in the open channel. It provides a versatile method for tuning an interatomic interaction strength by controlling the energy difference between the two states via a magnetic field or a photon [1]. The magnetic and optical tuning of FRs are called magnetic Feshbach resonance (MFR) [1] and optical Feshbach resonance (OFR) [2–4], respectively. MFRs are widely used in experiments of dilute quantum gases with alkali-metal atoms [1]. Even though the utility of OFRs with alkali-metal atoms can be limited compared to that of MFRs, OFRs provide an experimental means to tune the interatomic interaction strengths with various atomic species [5–8]. To date, OFRs have been used to generate bound molecules in the excited state, study asymptotic physics, and control forbidden molecular states [9,10]. Applications of OFRs also include tools for eliminating double occupancies in optical lattices [11–13].

OFRs have several advantages compared to their more established counterparts, MFRs. First, OFRs are available for all atomic species, including combinations of different atomic species [6]. Furthermore, OFRs can be manipulated in a much faster time scale than MFRs controlled by magnetic fields [14]. Finally, scattering lengths can be spatially modulated with high spatial frequency within a small atomic cloud [15].

Ytterbium (Yb) and strontium (Sr) atoms are special candidates for OFRs because they have the intercombination transitions whose linewidths are sub-MHz, substantially narrower than those of alkali-metal atoms. It has been suggested that OFRs with narrow-linewidth transitions can increase scattering lengths with relatively low atom loss [16]. Hence, bound molecules in the excited state have been generated with Yb and Sr atoms, which have optically accessible narrow-linewidth transitions [17–19]. Recently, atom-molecule conversion using an ultranarrow transition $^1S_0$-$^3P_2$ of ^{171}Yb atoms was also reported [20]. Furthermore, manipulation of the interatomic interaction has been conducted [7,8,14,15,21–23]. The OFRs of ^{88}Sr atoms with the intercombination transition have been well characterized with photoassociation (PA) spectroscopy of thermal gas experimentally and theoretically [8,14,18]. While the interatomic potential in the excited state and its molecular bound states of $^{174}Yb_2$ are well studied to date [21,24,25], quantitative measurements depending on PA intensities and frequencies regarding the OFRs of ^{174}Yb atoms are still required, including comparisons with theoretical calculations.

In this paper, we measure the OFRs of ^{174}Yb atoms in a pure BEC using the intercombination transition. The parameters characterizing these OFRs are studied with respect to PA laser intensities and frequencies. Theoretical calculations using a reflection approximation [2,26,27] are also performed and compared with the experimental results. The intensity dependence of the OFRs of ^{174}Yb atoms are reported. The measurements are performed with PA spectroscopy of a pure ^{174}Yb Bose-Einstein condensate (BEC). The high atom number density of a BEC provides orders of magnitude advantages in terms of the PA measurement signal-to-noise ratio compared to that of thermal atoms [4]. Also, the low temperatures of a BEC suppress the thermal broadening effect preventing asymmetric redshifts in the PA spectrum [8,18]. As a result, by using a BEC as a platform to study OFRs, we are able to clearly observe its dependance on the PA beam intensity and frequency. In addition to spectral measurements, we obtain temporal decay measurement of a pure BEC with PA processes to confirm our measurements. These measurements are done in the vicinity of the fourth vibrational level from the dissociation limit where effects from the single atom transition are negligible. The results acquired from the PA spectra and the temporal measurements are consistent.

This paper is organized as follows. Section II describes the experimental setup and the procedures for measuring the OFRs in a pure BEC of ^{174}Yb atoms near the intercombination transition. Section III outlines how we describe OFRs observed in experimentally measured PA spectra via isolated resonance model. Finally, Sec. IV provides a summary and an outlook for potential applications of OFRs.

II. EXPERIMENT

The experiment starts with a thermal beam of Yb atoms being decelerated by a Zeeman slower using the strong singlet transition ($^1S_0$-$^1P_1$, 398.9 nm). The ytterbium atoms exiting the Zeeman slower are captured with the core-shell magneto-optical trap (MOT) scheme [28]. The atoms trapped in the

*jcmun@kriss.re.kr

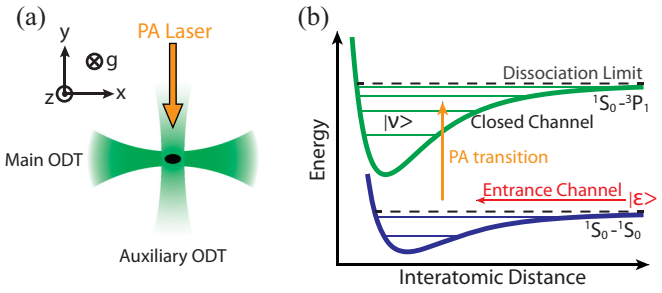

FIG. 1. (a) Schematic drawing of the crossed ODT and the PA laser. The two optical dipole traps are overlapped orthogonally on xy plane. The PA laser is co-aligned with the auxiliary ODT and is linearly polarized. (b) The energy diagram of interatomic molecular potentials of ground and excited states with their vibrational levels. Two atoms colliding in the entrance channel, $|\epsilon\rangle$, are coupled to a vibrational level, $|\nu\rangle$, in the closed channel via PA transition.

MOT are compressed and loaded into a 532-nm crossed optical dipole trap (ODT) that consists of two ODT arms, main and auxiliary. Figure 1(a) shows the crossed ODT configuration with respect to the PA laser beam. The main and the auxiliary ODTs overlap orthogonally in the xy plane at the center of the compressed MOT. Nine watts of laser power with a 532-nm wavelength is focused to construct the main ODT beam with a beam waist of 17 μm. The auxiliary ODT is made with a focused 30-μm beam waist having 1 W of optical power. A BEC of ^{174}Yb atoms is prepared in the crossed ODT after 4-s evaporation cooling. Subsequently, the auxiliary ODT power is increased by 15% to tighten the BEC. The atom number of a typical BEC is $N \approx 7 \times 10^4$ and its condensate fraction is more than 90%. The trapping frequencies of the crossed ODT are $(\omega_x,\omega_y,\omega_z) = 2\pi \times [130(5),184(7),225(9)]$ Hz during the PA process.

The interatomic molecular potential is depicted in Fig. 1(b), whose asymptote is the intercombination transition in the dissociation limit. A PA laser beam with a wavelength of 555.8 nm and a 600(5)-μm beam diameter was applied to a BEC with a Thomas-Fermi radius of $R_{\rm TF} = 3.7$ μm. The PA laser is linearly polarized along the z direction with less than 5-kHz laser linewidth. The frequency and beam intensity of the PA laser was controlled by a double-pass acousto-optic modulator. The beam intensity was stabilized before entering the vacuum chamber. The PA beam was applied to the condensate with low intensities, less than a saturation intensity of the intercombination transition ($0.14\,\mathrm{mW/cm^2}$), to reduce power broadening. The application durations ($4 \sim 20$ ms) of the PA beam were chosen such that the depletion of the condensate at the vibrational resonance of interest was well resolved but not saturated. Subsequently, both the PA laser beam and the crossed ODT were turned off simultaneously. After 18 ms of free expansion, measurements were taken via absorption imaging using a 398.9-nm laser resonant with the ground to singlet state ($^1S_0$-$^3P_1$). The atom loss in the trap due to background gas (lifetime >10 s) was negligible for the time scales of our experiments, <20 ms. Therefore, we were able to ignore the one-body loss contribution of the background gas in a BEC.

III. OPTICAL FESHBACH RESONANCE

A. Isolated resonance model

The isolated resonance model has been used to calculate various properties of the OFRs [3,29] showing good agreement with previous experimental results [7,8,14,15,17–19,21–23]. The model assumes that the molecular linewidths of the vibrational levels are negligibly small compared to the frequency spacings of the molecular resonances. Then, the OFRs can be described with the *optical length* and the *enhanced linewidth* of the vibrational level in the vicinity of a molecular resonance. The optical length represents the optical coupling strength between the scattering state in the entrance channel and a vibrational level in the closed channel. The optical length is defined as

$$l_{\rm opt} = \frac{3\lambda^3}{16\pi c}\frac{|\langle\nu|\epsilon\rangle|^2}{k} f_{\rm rot} I, \tag{1}$$

where $|\langle\nu|\epsilon\rangle|^2$ is the Franck-Condon factor corresponding to the vibrational level $|\nu\rangle$ in the closed channel and the energy normalized scattering state $|\epsilon\rangle$ in the entrance channel. $f_{\rm rot} = 1/3$ is the rotational factor, $\lambda = 555.8$ nm is the wavelength of the intercombination transition $^1S_0$ -$^3P_1$, $k = \sqrt{21/8}/(2R_{\rm TF})$ is a wave number for a BEC, and I is the PA laser intensity. In the ultracold regime, $|\langle\nu|\epsilon\rangle|^2$ is proportional to the wave number by the threshold law for s-wave collisions. Therefore, the optical length per intensity, $l_{\rm opt}/I$, can be treated as a constant for a given OFR [4,8,14]. The enhanced linewidth is the broadened molecular linewidth induced by an artificial channel that accounts for the spontaneous emission or other trap loss processes [30].

Experimentally, $l_{\rm opt}$ and the enhanced linewidth of the vibrational level can be acquired using PA spectroscopy [4,31]. According to the isolated resonance model, the optically induced scattering length $a_{\rm opt}$ and the two-body loss rate K_2 of the vibrational level are given as

$$a_{\rm opt} = \frac{l_{\rm opt}\Gamma_{\rm mol}\Delta}{\Delta^2 + (\eta\Gamma_{\rm mol})^2/4}, \tag{2}$$

$$K_2 = \frac{2\pi\hbar}{\mu}\frac{\eta\Gamma_{\rm mol}^2 l_{\rm opt}}{\Delta^2 + (\eta\Gamma_{\rm mol} + \Gamma_{\rm stim})^2/4}, \tag{3}$$

where $\eta\Gamma_{\rm mol}$ is the enhanced linewidth expressed via the molecular linewidth, $\Gamma_{\rm mol} = 2\pi \times 364$ kHz and the enhanced factor $\eta > 1$. $\Gamma_{\rm stim} = 2kl_{\rm opt}\Gamma_{\rm mol}$ is the stimulated linewidth induced by the PA beam intensity. Δ is the PA laser detuning with respect to the vibrational resonance, $\mu = m/2$ is the reduced mass for the atomic mass m of ^{174}Yb. The linewidth enhancement of vibrational levels, characterized by η [2,14], has been observed in previous experiments [6,8,18,23]. $\Gamma_{\rm stim}$ acts as an additional source of power broadening of the molecular linewidth due to the applied PA laser. In the low-intensity regime of the PA laser, $\Gamma_{\rm stim}$ can be ignored [14,15].

The PA process leads to a two-body loss mechanism when applied to a BEC. Two colliding atoms absorb a photon resonant at the vibrational level and forms a molecule in the excited state. The molecule decays due to spontaneous emission, which results in atom loss in the BEC which is measured after free expansion. The two-body loss of a BEC

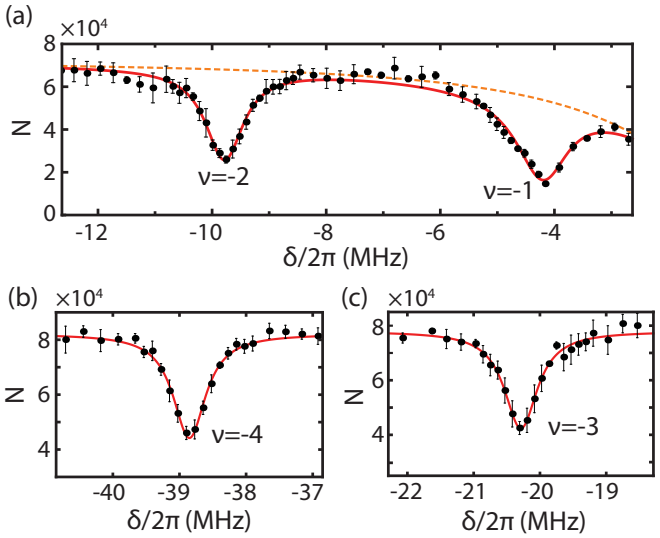

FIG. 2. PA spectra of four least-bound vibrational levels near the intercombination transition, $\nu = -1, -2, -3$, and -4. The applied PA beam intensity is 71.5(2) μW/cm^2 and $t_{\rm PA}$ are (a) 4 ms, (b) 9 ms, and (c) 4 ms. N is the remaining atom number after the PA process. δ is the angular frequency detuning from the atomic resonance. The error bars represent 1-σ bounds for the statistical errors. The red solid lines in the spectra represent the fit result using Eq. (5). The dashed orange line represents atom loss due to the atomic intercombination transition ($K_{\rm res}$).

can be described by the following rate equation [32]:

$$\frac{d}{dt}\ln N = -K_2 C_2 N^{2/5}, \tag{4}$$

where $C_2 = 15^{2/5}/14\pi\,[m\bar{\omega}/(\hbar\sqrt{a_{\rm bg}})]^{6/5}$ with $\bar{\omega} = (\omega_x\omega_y\omega_z)^{1/3} = 175(7)$ Hz. $\hbar$ is the reduced Planck constant, and $a_{\rm bg} = 5.55(8)$ nm [33] is the background scattering length of ^{174}Yb.

Yan *et al.* [23] found that the modification of the atom loss due to PA laser intensity well describes the measurements near the atomic resonance by adding the atom loss rate due to the atomic resonance, $K_{\rm res}$, to K_2, where $K_{\rm res} = K_0(\Gamma_{\rm mol}/\delta)^2/4$. K_0 is the decay constant at the atomic resonance, and δ denotes the detuning from the atomic resonance. Following their phenomenological approach to include one-body loss due to the atomic resonance into the two-body loss term, we simplify the data analysis separating out the molecular peaks ($K_{2,\nu}$ term from each molecular state ν) from the atomic resonance background spectrum [$K_{\rm res}$, orange dashed line in Fig. 2(a)]. Note that the $K_{\rm res}$ contribution becomes negligible in the measurements of vibrational levels far from the atomic resonance [Figs. 2(b) and 2(c)]. With this modification, we can extract the information of the molecular spectra near the atomic resonance.

Combining the analytic solution of Eq. (4) with the two-body loss rate in Eq. (3) and $K_{\rm res}$, the atom loss spectrum is given as

$$N = N_0\left[1 + \tfrac{2}{5}t_{\rm PA}N_0^{2/5}C_2(K_2 + K_{\rm res})\right]^{-5/2}, \tag{5}$$

where N_0 is the initial atom number of the BEC, and $t_{\rm PA}$ is the PA beam application time.

B. Photoassociation

With various PA beam intensities, we characterize $l_{\rm opt}$ and η associated with the four least-bound vibrational levels near the intercombination transition. The PA application time $t_{\rm PA}$ was chosen such that about half of the initial number of atoms was lost from the trap at a given molecular resonance. The PA spectra were taken by scanning the frequency of the PA laser.

Figures 2(a)–2(c) show the PA spectra of four least-bound vibrational levels. The negative indices of the vibrational levels are labeled from the dissociation limit. Each spectrum is an average of four independent scans. The red solid lines of Fig. 2 are acquired by fitting each PA spectrum with Eq. (5). The orange dashed line of Fig. 2(a) represents atom loss due to the atomic resonance. We consider $K_{\rm res}$ when performing the fits for the PA spectra of $\nu = -1$ and $\nu = -2$ because the atom loss due to the atomic resonance affects the two vibrational levels. Note that we do not need to include $K_{\rm res}$ for the cases of $\nu = -3$ and $\nu = -4$ where it is negligible. The symmetric line shape of each molecular resonance shows that the thermal broadening observed in other thermal gas experiments is absent in this work [4,8,18,25]. $l_{\rm opt}$, η, and the resonance frequencies of the vibrational levels are measured with the PA spectra for a range of PA beam intensities. $\Gamma_{\rm stim}$ of each vibrational level is less than 20 Hz, which satisfies the condition for the low-intensity regime. Hence, we ignore $\Gamma_{\rm stim}$ in Eq. (3) for our analysis.

Figure 3 shows the measured $l_{\rm opt}$ and η of each vibrational level for various intensities. The solid lines shown in Figs. 3(a) and 3(b) are the linear fits of $l_{\rm opt}$ with respect to the PA beam intensity. The dashed lines in Figs. 3(c) and 3(d) show the average values of η for the range of applied PA beam intensities. The uncertainty of C_2 affected by those of $a_{\rm bg}$ and $\bar{\omega}$ are considered when we acquire the fit errors of $l_{\rm opt}$ and η. The uncertainties of PA beam intensity, $l_{\rm opt}$, and η are considered for the linear and constant fits in Fig. 3. The data clearly show that $l_{\rm opt}/I$, shown as the slope values in Figs. 3(a) and 3(b), can be treated as a constant in the ultracold regime [2]. The data show that η is independent of the PA laser intensity, which was not shown in previous experiments [8,23]. Thus, we treat this broadening as a local parameter of the vibrational level. Within the range of our experimental parameters, we did not observe noticeable deviation from the linear dependence of $l_{\rm opt}$ due to the Stark effect induced by the PA laser beam, which has been reported previously [34]. We estimate that the frequency shifts of the four vibrational levels due to the PA laser intensity are less than 10 Hz in our experiment.

The experimental results and theoretical calculations of the OFR parameters are summarized in Table I. Theoretical values of $l_{\rm opt}/I$ are calculated using the reflection approximation [2,26,27] with the intermolecular potentials in Ref. [25] and the dipole matrix element of the intermolecular state. $l_{\rm opt}/I$ of ^{174}Yb atoms are larger than those of ^{88}Sr atoms in Ref. [8] because ytterbium atoms have larger dipole moments of the intercombination transition than that of strontium atoms. Also, the calculation and measurements of $l_{\rm opt}/I$ show that more deeply bound molecular states have smaller $l_{\rm opt}/I$. Yamazaki *et al.* [15] calculated and measured $l_{\rm opt}$ of ^{174}Yb for

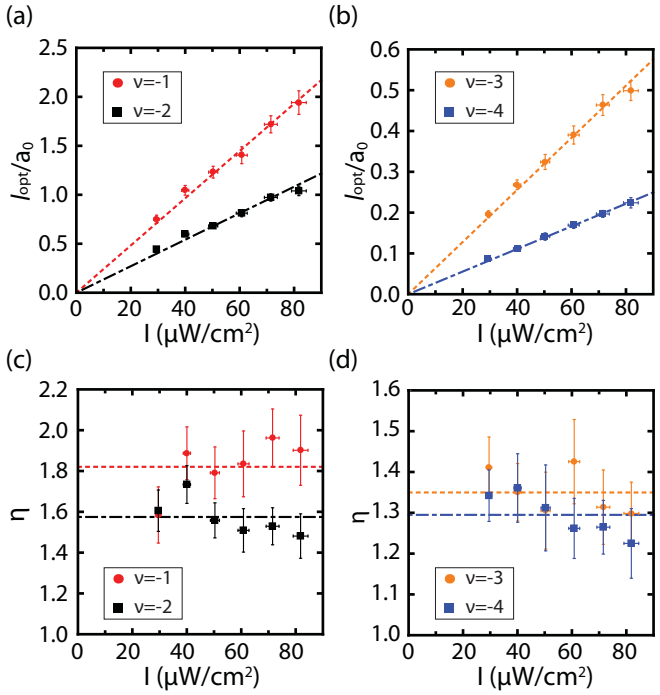

FIG. 3. Measurement of optical length l_{opt} [(a) and (b)], and enhanced factors η [(c) and (d)] of the bound states of $\nu = -1$ (red circle), -2 (black square), -3 (orange circle). and -4 (blue square) with various PA intensities. The dashed and double dashed lines in (a) and (b) are linear fits of the data points of l_{opt}, while dashed and double dashed lines in (c) and (d) show the mean of η data points. a_0 is the Bohr radius.

$\nu = -5, -6, -7$, where the same tendencies were reported. The discrepancy between our theoretical and experimental values in Table I might originate from our theoretical model approximation that the molecular dipole matrix element that depends on the interatomic distance is assumed to be a constant dipole matrix element for the atomic transition. The molecular dipole matrix element converges to that of the atomic transition as the Condon point, which corresponds to the classical turning point for the molecular potential, approaches infinity. However, the molecular dipole matrix element actually deviates from the atomic transition value as the molecular binding becomes deeper, resulting in noticeable

TABLE I. PA resonances frequencies, l_{opt}/I, and η for each vibrational level. The resonance frequencies f_ν are defined from the dissociation limit. The parentheses for values of l_{opt}/I, f_ν, and η are 1-σ statistical errors.

	Theory	Experiment		
ν	l_{opt}/I $\left(10^3 \frac{a_0}{\mathrm{W/cm^2}}\right)$	l_{opt}/I $\left(10^3 \frac{a_0}{\mathrm{W/cm^2}}\right)$	f_ν (MHz)	η
-1	20.1	24.1(12)	$-4.18(2)$	1.82(6)
-2	10.4	13.5(10)	$-9.78(2)$	1.57(4)
-3	7.4	6.39(29)	$-20.28(2)$	1.35(3)
-4	5.2	2.77(7)	$-38.87(2)$	1.30(3)

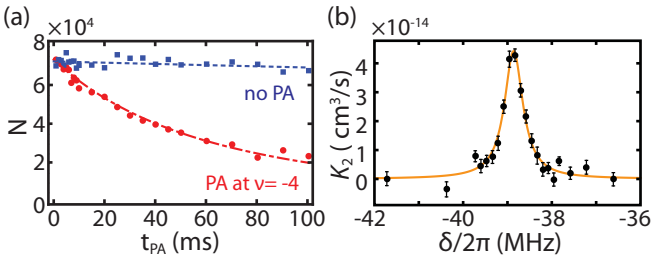

FIG. 4. (a) Typical temporal decay of the BEC atom number with (red circle) and without (blue square) the PA beam resonant at $\nu = -4$. The red double dashed and blue dashed lines are the two-body loss fits with and without PA beam, respectively. The PA beam intensity is 20.8(1) μW/cm^2. (b) The two-body loss measured via temporal measurements of the BEC for various δ near $\nu = -4$. The orange solid line is a fit of the two-body loss using Eq. (3).

mismatch between our numerical estimates and measurement especially for the cases of higher ν.

To confirm the experimentally obtained parameters in Table I, we measured the two-body loss rate by monitoring the temporal decay of a BEC after applying a PA beam near the resonance at $\nu = -4$. Figure 4(a) shows the typical temporal decay of a BEC with and without a PA beam resonant at $\nu = -4$. The PA beam intensity was 20.8(1) μW/cm^2. The data was taken via independent experiments with varying t_{PA}. Each point is an average of four measurements. The dashed red and blue double dashed lines represent the corresponding fit results of the temporal decay according to Eq. (4). We measured the two-body loss rate K_2 with respect to various PA laser frequencies near $\nu = -4$. Data points in Fig. 4(b) represent an average of four measurements of the two-body loss rate. The error bars depict 1-σ statistical errors. The orange solid line in Fig. 4(b) is the fit result of two-body loss rate using Eq. (3). We acquired $l_{opt}/I = 3.02(16) \times 10^3 a_0/(\mathrm{W/cm^2})$ and $\eta = 1.39(8)$ from the two-body loss fit in Fig. 4(b). l_{opt}/I and η are measured to be slightly greater than the values in Table I by less than 10%. This result shows that OFR measurements using PA spectroscopy give results comparable to time-dependent measurements of the two-body loss rate.

IV. SUMMARY AND CONCLUSION

In conclusion, we have measured the optical Feshbach resonances of ^{174}Yb atoms in a pure BEC via PA spectroscopy with the intercombination transition. It is shown that the optical length has linear dependance on the PA beam intensity and the enhanced factors are independent of the intensity within the parameter range of our experiments. These results enable us to better understand the molecular potentials and wave functions of the bound molecular states of ^{174}Yb$_2$. OFRs of two-electron atoms, such as Yb and Sr, can extend the bounds of many experiments due to their nonsusceptibility to external magnetic fields. These types of systems have the potential to overcome the drawbacks associated with magnetic Feshbach resonances, which have interaction strengths that are difficult to control due to stray magnetic fields. The measured parameters of OFRs in this work allow us to calculate the optically induced scattering lengths and two-body loss rates that were not previously available.

ACKNOWLEDGMENTS

We thank Eunmi Chae for helpful discussions. This research was supported by Korea Research Institute of Standards and Science (KRISS) creative research initiative, the R&D Convergence Program of NST (National Research Council of Science and Technology) of the Republic of Korea (Grant No. CAP-15-08-KRISS), and IBS-R009-D.

[1] C. Chin, R. Grimm, P. Julienne, and E. Tiesinga, Rev. Mod. Phys. **82**, 1225 (2010).
[2] J. L. Bohn and P. S. Julienne, Phys. Rev. A **60**, 414 (1999).
[3] P. O. Fedichev, Y. Kagan, G. V. Shlyapnikov, and J. T. M. Walraven, Phys. Rev. Lett. **77**, 2913 (1996).
[4] K. M. Jones, E. Tiesinga, P. D. Lett, and P. S. Julienne, Rev. Mod. Phys. **78**, 483 (2006).
[5] C. McKenzie, J. Hecker Denschlag, H. Häffner, A. Browaeys, L. E. E. de Araujo, F. K. Fatemi, K. M. Jones, J. E. Simsarian, D. Cho, A. Simoni, E. Tiesinga, P. S. Julienne, K. Helmerson, P. D. Lett, S. L. Rolston, and W. D. Phillips, Phys. Rev. Lett. **88**, 120403 (2002).
[6] M. Theis, G. Thalhammer, K. Winkler, M. Hellwig, G. Ruff, R. Grimm, and J. H. Denschlag, Phys. Rev. Lett. **93**, 123001 (2004).
[7] K. Enomoto, K. Kasa, M. Kitagawa, and Y. Takahashi, Phys. Rev. Lett. **101**, 203201 (2008).
[8] S. Blatt, T. L. Nicholson, B. J. Bloom, J. R. Williams, J. W. Thomsen, P. S. Julienne, and J. Ye, Phys. Rev. Lett. **107**, 073202 (2011).
[9] B. H. McGuyer, M. McDonald, G. Z. Iwata, M. G. Tarallo, W. Skomorowski, R. Moszynski, and T. Zelevinsky, Nat. Phys. **11**, 32 (2015).
[10] B. H. McGuyer, M. McDonald, G. Z. Iwata, W. Skomorowski, R. Moszynski, and T. Zelevinsky, Phys. Rev. Lett. **115**, 053001 (2015).
[11] T. Akatsuka, M. Takamoto, and H. Katori, Phys. Rev. A **81**, 023402 (2010).
[12] S. Sugawa, K. Inaba, S. Taie, R. Yamazaki, M. Yamashita, and Y. Takahashi, Nat. Phys. **7**, 642 (2011).
[13] K. Shibata, R. Yamamoto, Y. Seki, and Y. Takahashi, Phys. Rev. A **89**, 031601 (2014).
[14] T. L. Nicholson, S. Blatt, B. J. Bloom, J. R. Williams, J. W. Thomsen, J. Ye, and P. S. Julienne, Phys. Rev. A **92**, 022709 (2015).
[15] R. Yamazaki, S. Taie, S. Sugawa, and Y. Takahashi, Phys. Rev. Lett. **105**, 050405 (2010).
[16] R. Ciuryło, E. Tiesinga, and P. S. Julienne, Phys. Rev. A **71**, 030701 (2005).
[17] S. Kato, R. Yamazaki, K. Shibata, R. Yamamoto, H. Yamada, and Y. Takahashi, Phys. Rev. A **86**, 043411 (2012).
[18] T. Zelevinsky, M. M. Boyd, A. D. Ludlow, T. Ido, J. Ye, R. Ciuryło, P. Naidon, and P. S. Julienne, Phys. Rev. Lett. **96**, 203201 (2006).
[19] G. Reinaudi, C. B. Osborn, M. McDonald, S. Kotochigova, and T. Zelevinsky, Phys. Rev. Lett. **109**, 115303 (2012).
[20] S. Taie, S. Watanabe, T. Ichinose, and Y. Takahashi, Phys. Rev. Lett. **116**, 043202 (2016).
[21] S. Tojo, M. Kitagawa, K. Enomoto, Y. Kato, Y. Takasu, M. Kumakura, and Y. Takahashi, Phys. Rev. Lett. **96**, 153201 (2006).
[22] M. Yan, B. J. DeSalvo, Y. Huang, P. Naidon, and T. C. Killian, Phys. Rev. Lett. **111**, 150402 (2013).
[23] M. Yan, B. J. DeSalvo, B. Ramachandhran, H. Pu, and T. C. Killian, Phys. Rev. Lett. **110**, 123201 (2013).
[24] K. Enomoto, M. Kitagawa, K. Kasa, S. Tojo, and Y. Takahashi, Phys. Rev. Lett. **98**, 203201 (2007).
[25] M. Borkowski, R. Ciuryło, P. S. Julienne, S. Tojo, K. Enomoto, and Y. Takahashi, Phys. Rev. A **80**, 012715 (2009).
[26] P. S. Julienne, J. Res. Natl. Inst. Stand. Technol. **101**, 487 (1996).
[27] R. Ciuryło, E. Tiesinga, and P. S. Julienne, Phys. Rev. A **74**, 022710 (2006).
[28] J. Lee, J. H. Lee, J. Noh, and J. Mun, Phys. Rev. A **91**, 053405 (2015).
[29] J. L. Bohn and P. S. Julienne, Phys. Rev. A **56**, 1486 (1997).
[30] M. L. Du and A. Dalgarno, Phys. Rev. A **43**, 3474 (1991).
[31] R. Ciuryło, E. Tiesinga, S. Kotochigova, and P. S. Julienne, Phys. Rev. A **70**, 062710 (2004).
[32] J. Söding, D. Guéry-Odelin, P. Desbiolles, F. Chevy, H. Inamori, and J. Dalibard, Appl. Phys. B **69**, 257 (1999).
[33] M. Kitagawa, K. Enomoto, K. Kasa, Y. Takahashi, R. Ciuryło, P. Naidon, and P. S. Julienne, Phys. Rev. A **77**, 012719 (2008).
[34] I. D. Prodan, M. Pichler, M. Junker, R. G. Hulet, and J. L. Bohn, Phys. Rev. Lett. **91**, 080402 (2003).